The Canadian Mineralogist
Vol. 58, pp. 1-14 (2020)
DOI: 10.3749/canmin.1900106

THE PHOSPHATE MINERAL ASSEMBLAGES FROM LA VIQUITA PEGMATITE, SAN LUIS, ARGENTINA

MIGUEL A. GALLISKI[§]

IANIGLA, CCT-Mendoza CONICET, Av. Ruiz Leal s/n, Parque Gral. San Martín; C.C.330 (5.500) Mendoza, Argentina

ENCARNACIÓN RODA-ROBLES

Departamento de Mineralogía y Petrología, Universidad del País Vasco, UPV/EHU, Spain

FRÉDÉRIC HATERT

Laboratory of Mineralogy B18, University of Liège, B-4000 Liège, Belgium

MARÍA FLORENCIA MÁRQUEZ-ZAVALÍA

IANIGLA, CCT-Mendoza, CONICET, Av. Ruíz Leal s/n, Parque Gral. San Martín; C.C.330 (5.500) Mendoza, Argentina
Mineralogía y Petrología, FAD, Universidad Nacional de Cuyo. (5500) Mendoza, Argentina

VIVIANA A. MARTÍNEZ

Departamento de Geología, FCEyN, Universidad Nacional de La Pampa, Argentina

ABSTRACT

La Viquita is a rare-element pegmatite of LCT signature, REL-Li subclass, spodumene subtype, that shows Fe > Mn mineral paragenesis instead of Mn > Fe, which is more common in the rare-element pegmatite population of the San Luis ranges. The phosphate mineral association of this pegmatite can be subdivided into (1) primary, with dendritic triphylite [(Fe/(Fe + Mn) = 0.72] and montebrasite–amblygonite as main phases; (2) metasomatic, with subsolidus replacement of triphylite by ferrisicklerite and heterosite; and (3) hydrothermal, with secondary growth of alluaudite at the expense of heterosite and wardite from montebrasite caused by Na-metasomatism. A Ca-rich influx under oxidizing conditions produced childrenite–eosphorite–ernstite, jahnsite-(CaMnFe), and kingsmountite. Apatite-group minerals are present throughout the processes. Very late-stage solutions formed millimetric crystals of hydroxylherderite associated with hydroxylapatite in cavities in K-feldspar.

Keywords: phosphate derivatives, triphylite, montebrasite, pegmatite, LCT, Argentina.

INTRODUCTION

Accessory Fe-Mn (±Li,Al,Na) and Li-Al (±Ca,Na) phosphate nodules are common in the LCT (Li-Cs-Ta) rare-element pegmatites of the San Luis Ranges, Argentina, located in the southern part of the large Pampean Pegmatite Province of Paleozoic age. Most of these phosphates occur in pegmatites of the beryl type and spodumene subtype. As is common in other pegmatite fields throughout the world, the primary assemblages are not very complex, consisting of members of the series triphylite–lithiophilite, graftonite–beusite, triplite–zwieselite, amblygonite–montebrasite, and rarely qingheiite (Galliski *et al*. 2009), bobfergusonite (Tait *et al*. 2004), or dickinsonite. The altered species form secondary metasomatic or hydrothermal assemblages that are mineralogically more complex and normally shed light on the conditions of

§ *Corresponding author e-mail address*: galliski@mendoza-conicet.gov.ar

the subsolidus transformation processes. These assemblages take various forms as seen in, for example, pegmatite fields in Sweden (Quensel 1937, Mason 1941, Smeds *et al*. 1998), Spain (Roda-Robles *et al*. 1996, 1998, 2004, 2010), Poland (Wlodek *el al*. 2015), Africa (Fransolet 1980, Fransolet *et al*. 1986, Keller 1988, Keller & von Knorring 1989, Keller *et al*. 1994), Canada (Černý *et al*. 1998), EEUU (Moore 1973, Nizamoff 2006), and Brasil (Baijot *et al*. 2012, 2014). The study of these assemblages contributes to the knowledge about the origin and evolution of some accessory phosphate minerals from rare-element pegmatites. In this contribution we describe the phosphates occurring in La Viquita, a spodumene subtype, complex rare-element pegmatite of the Rare-Element-Li (REL-Li) class according to the classification of Černý & Ercit (2005).

Geology of the Pegmatite

The La Viquita pegmatite is located in the La Estanzuela range, at 65°06′39.79″ W and 32°51′25.60″ S, in the Chacabuco Department, San Luis Province, Argentina. Its general geology was described by Angelelli & Rinaldi (1963) and more recently by Martínez & Galliski (2000) and Galliski *et al*. (2008). The host rock of the pegmatite is a dark-grey quartz-biotite-muscovite-plagioclase schist, with sporadic occurrences of staurolite and garnet porphyroblasts in the surroundings of the body, belonging to the Conlara Metamorphic complex of Lower Paleozoic age (Sims *et al*. 1997). What appears to be the upper part of the pegmatite is partially exposed in an open pit. The internal structure visible in outcrop shows approximately concentric zoning that consists of border, wall, intermediate, and quartz core zones (Fig. 1). The border zone, which reaches a thickness of up to 7 cm, is composed of a fine-grained intergrowth of quartz and muscovite. It is followed inward by a wall zone up to 1 m thick composed of a medium- to fine-grained K-feldspar-quartz-albite and muscovite assemblage, with garnet, tourmaline, beryl, columbite-group minerals, and Fe-Mn phosphates as accessory phases, and secondary Fe-Mn oxides (Fig. 2a). The intermediate zone is subdivided into outer, middle, and inner subzones: all of these are coarse-grained and dominated by K-feldspar-quartz-albite. The K-feldspar proportion diminishes from up to 70% in the outer subzone to up to 30% in the inner subunit. Albite and spodumene modal proportions increase inward from 25% and 1% up to 30% and 15–20 vol.% albite and spodumene, respectively, in the inner intermediate zone. These subunits contain accessory muscovite, beryl, decametric-sized nodules of montebrasite, nodules of members of the triphylite–lithiophilite series in the outer subzone, and minor apatite supergroup minerals, childrenite–eosphorite aggregates, columbite-group minerals, wodginite-group minerals, and cassiterite (Galliski *et al*. 2008). The core of the pegmatite is composed of quartz, spodumene, minor K-feldspar, and traces of pyrite. In general, the decimetric olive-gray crystals of spodumene are moderately to highly altered. Besides the Fe-Mn phosphates described in this paper, up to 40 cm-diameter nodules of predominantly montebrasite are common. Late-stage millimeter-sized crystals of hydroxylherderite partially covered by hydroxylapatite are occasionally found lining small cavities in the core margin association where an assemblage containing adularia and albite, scarce quartz, fluorapatite, and minor flakes of muscovite has been described (Černý *et al*. 2011). From the geochemical point of view, La Viquita is a relatively Fe-enriched pegmatite, which differs from other pegmatite occurrences of the San Luis ranges, where the dominance of Mn over Fe is common in the primary phosphate associations.

Methodology

Sampling of the wall zone of the La Viquita pegmatite was carried out at the quarry entrance, while the intermediate zones were sampled from different parts of the quarry walls (Fig. 1). In one of our visits we found a small exposure of fresh phosphates from the intermediate zone. The minerals were identified and their textural relationships were described using thin sections and a polarizing microscope. Most of the chemical analyses were performed with a Cameca SX50 electron microprobe at the Université Paul Sabatier (Toulouse, France). The operating conditions were: voltage 15 kV, beam current 10 nA. The internal standards used for the phosphates were natural minerals except for Pb; unless otherwise specified, $K\alpha$ lines were used: P (graftonite), Al (corundum), Fe (hematite), Mn (pyrophanite), Mg (periclase), Ca and Si (wollastonite), K (sanidine), Na (albite), S (celestine), Ba$L\alpha$ (barite), and Pb$M\beta$ ($Pb_2P_2O_7$).

Additional chemical analyses were performed with a CAMECA SX100 electron microprobe in the Microprobe Laboratory of Masaryk University and the Czech Geological Survey (Brno, Czech Republic). The operating conditions were: acceleration potential of 15 kV, sample current of 10 nA measured on a Faraday cup, and beam diameter of 5 μm. The counting time on peaks was 30 s for Si and F; 20 s for Ti, Zn, Sr, and Ba; 10 s for the rest of the elements; and half of the peak time on the high and low backgrounds. The standards and analytical lines selected ($K\alpha$) were: P, Ca (fluorapatite), Si, Mn

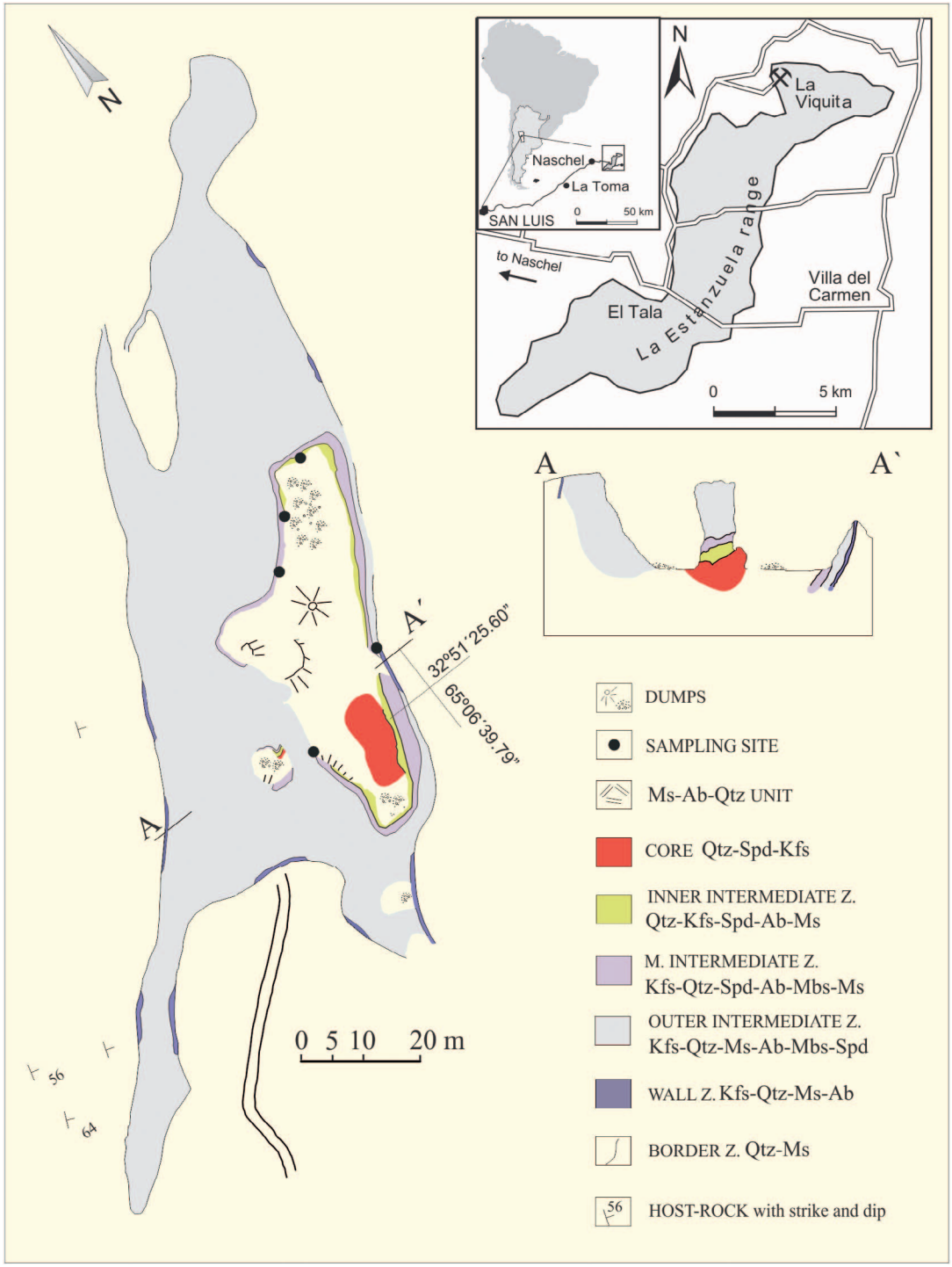

FIG. 1. Geological map of the La Viquita pegmatite and cross section showing the internal structure, modified after the map of Martínez & Galliski (2000), with locations of sampling sites. Symbols for rock-forming minerals are from Kretz (1983), plus mbs for montebrasite.

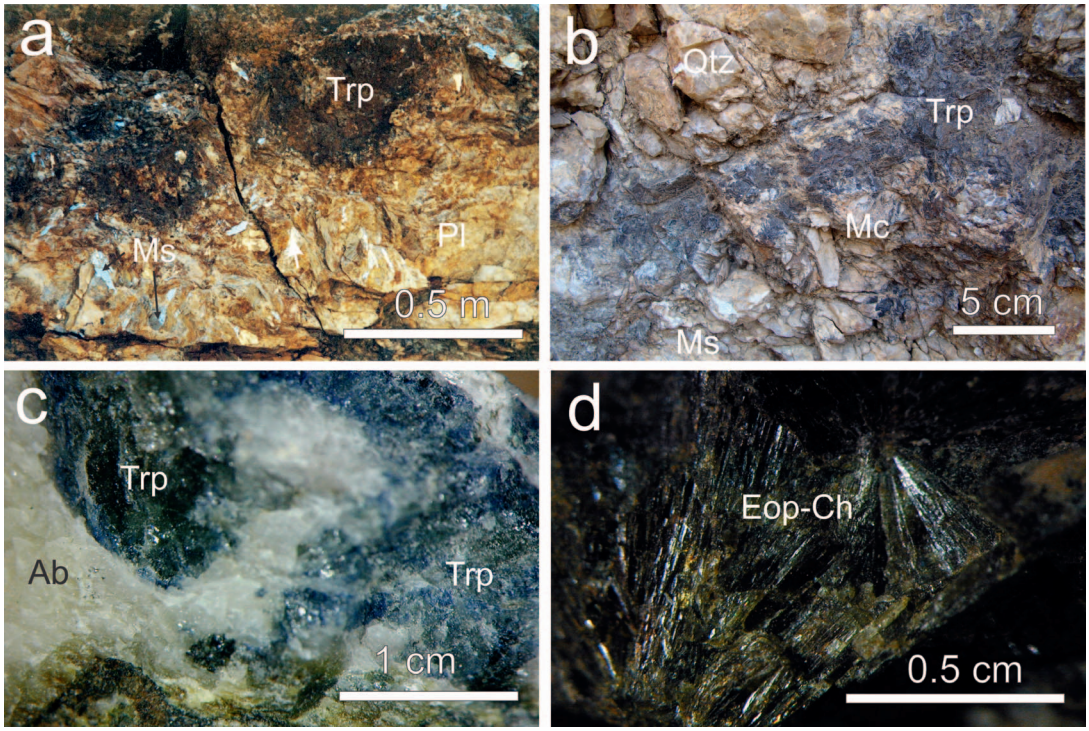

FIG. 2. Macro-mesoscopic photographs of phosphates from the La Viquita pegmatite. (a) Partially oxidized triphylite (Trp) nodules contained in a matrix of plagioclase, quartz (Qtz), and muscovite (Ms) in the wall zone. (b) Fresh dendritic triphylite contained in K-feldspar (Mc), quartz, and muscovite in the outer intermediate zone. (c) Blue massive triphylite associated with albite (Ab) in the intermediate zone. (d) Divergent crystals of eosphorite–childrenite (Eop–Ch) in aggregates in the intermediate zone.

(spessartine), Ti (titanite) Al, K (sanidine), Fe (hematite), Mg (Mg_2SiO_4), Zn (gahnite), Na (albite), and Cl (vanadinite). Fluorine, Sr, and Ba were sought but not found. Hydroxylherderite and apatite were analyzed at the Laboratorio de Microscopía Electrónica y Análisis por Rayos X (LAMARX), Universidad Nacional de Córdoba (Argentina), using a JEOL JXA 8230 Superprobe with a beam diameter of 10 μm and an acceleration potential of 15 kV. Analytical conditions included a sample current of 10 nA measured on a Faraday cup and counting times of 10 and 5 s for all elements and backgrounds, respectively, except for F and Na (5 and 2.5 s). The standards and analytical lines selected were: F (topaz $K\alpha$), Na, Si (albite $K\alpha$), Mg (MgO $K\alpha$), Ca (zoisite $K\alpha$), Mn (pyrolusite $K\alpha$), hematite (Fe $K\alpha$), P (libethenite $K\alpha$), and Sr (celestine $L\alpha$). The data were reduced using the PAP routine of Pouchou & Pichoir (1985). X-ray diffraction diagrams of powdered minerals were obtained with a Rigaku Denki DMax II-C instrument using Ni filtered Cu radiation ($\lambda = 1.54056$ Å) and operated at 40 kV and 30 mA at the Universities of Salta and San Luis.

THE PHOSPHATE ASSEMBLAGES

The chemical compositions and associations of the phosphates identified in the La Viquita pegmatite are given in Table 1. They can be subdivided into primary (considered magmatic), metasomatic formed by subsolidus replacement of primary minerals, and hydrothermal generated postmagmatically by late-stage solutions.

Triphylite $LiFe^{2+}(PO_4)$

The Li-Fe-Mn phosphates occur in several zones of the pegmatite. In the wall zone, triphylite is present in centimetric-sized dendritic and skeletal crystals which are grouped in up to 10 cm diameter irregular greenish brown nodules, commonly in an advanced state of alteration, intergrown with albite and minor muscovite, quartz, and tourmaline (Fig. 2a).

TABLE 1. PHOSPHATE MINERALS IDENTIFIED IN THE LA VIQUITA PEGMATITE

Species	Formula	Paragenesis
	Magmatic	
Triphylite	$LiFe^{2+}PO_4$	Pl-Ms-Mc-Qtz-Ap
Montebrasite	$LiAl(PO_4)(OH)$	Pl-Qtz-Mc-Ms-Sp
Fluorapatite	$Ca_5(PO_4)_3F$	Qtz-Pl-Mc-Ms
	Metasomatic	
Ferrisicklerite	$Li_{1-x}(Fe^{3+},Mn^{2+})(PO_4)$	
Heterosite	$Fe^{3+}(PO_4)$	Pl-Ms-Mc-Qtz-Trp
Alluaudite	$(Na,Ca)(Mn,Mg,Fe^{2+})(Fe^{3+},Mn^{2+})_2(PO_4)_3$	Pl-Ms-Mc-Qtz
	Hydrothermal	
Childrenite	$Fe^{2+}Al(PO_4)(OH)_2{\cdot}H_2O$	
Eosphorite	$Mn^{2+}Al(PO_4)(OH)_2{\cdot}H_2O$	
Ernstite	$(Mn^{2+}Fe^{3+})Al(PO_4)(OH,O)_2$	
Jahnsite-(CaMnFe)	$CaMn^{2+}Fe^{2+}{}_2Fe^{3+}{}_2(PO_4)_4(OH)_2{\cdot}8H_2O$	
Wardite	$NaAl_3(PO_4)_2(OH)_4{\cdot}2H_2O$	
Kingsmountite	$Ca_3MnFe^{2+}Al_4(PO_4)_6(OH)_4{\cdot}12H_2O$	
Hydroxylherderite	$CaBe(PO_4)(OH)$	Qtz-Ab-ApOH
Hydroxylapatite	$Ca_5(PO_4)_3OH$	

In the outer intermediate zone of the pegmatite, triphylite occurs in dispersed nodules up to 10–20 cm in diameter, but usually smaller. Most of these nodules are altered to a mass of secondary phosphates and black Mn-Fe oxides. Occasionally, they show fresh material with some color zoning, from blackish brown in the outer part to greenish inward. Crystals with a dendritic habit are also frequent (Figs. 2b, 3a). Exceptionally, after some sporadic period of mining of the pegmatite, one nodule found in the SW wall of the quarry showed fresh greenish blue triphylite in a groundmass of quartz + albite + K-feldspar + muscovite (Fig. 2c).

It was not possible to analyze the dendritic triphylite of the wall zone because fresh remnant patches of it were not found in the replacement mass of ferrisicklerite, but it is possible to infer its $Fe_t/(Fe_t + Mn)$ ratios because this secondary mineral mirrors them; they are in the range 0.717–0.682.

The chemical composition of the greenish blue triphylite (Table 2) shows Si replacement for P up to 0.012 atoms per formula unit (*apfu*), MgO wt.% contents up to 2.73, traces of Ca and Zn, and predominance of Fe over Mn with $Fe_t/(Fe_t + Mn)$ values averaging 0.72 (± 0.004), similar to the ferrisicklerite after triphylite. The empirical formula of fresh triphylite is $Li_{0.998}(Fe^{2+}{}_{0.637}Mn_{0.248}Mg_{0.100}Ca_{0.002}\ Zn_{0.002})(P_{0.992}Si_{0.008})O_4$.

Apatite supergroup minerals, $Ca_5(PO_4)_3F/Cl/OH$

Minerals from the apatite supergroup are well distributed in small quantities in both the primary and secondary assemblages of phosphates. The wall zone contains small, irregular crystals that show variable chemical compositions with MnO contents up to 4.60 wt.% and FeO up to 1.72 wt.%. In the intermediate zones they occur as small prismatic crystals included preferentially in albite and microcline. In both cases, based on the parageneses, the apatite is considered primary.

The secondary hydrothermal members of this supergroup are related to some small, centimeter-sized vugs in K-feldspar, coated by druses of euhedral, short prismatic to tabular crystals up to 2 mm long that cover morphologically similar crystals of hydroxylherderite and are usually associated with quartz and euhedral albite crystals. The chemical composition of these crystals shows up to 4.6 wt.% Mn and dominance of OH over Cl and F in the X-site.

In another late-stage association that occurs close to the assemblage of adularia-albite described by Černý *et al*. (2011), microcline, quartz, and muscovite present in cavities as euhedral crystals are sporadically covered by late-formed acicular millimetric fibro-radiate aggregates of tiny white crystals of apatite. The crystals of this last assemblage were not analyzed but by comparison with other similar occurrences in the Pampean pegmatites they could have predominant OH at the X site.

Amblygonite–montebrasite, $LiAl(PO_4)(F/OH)$

Montebrasite is widely distributed in the intermediate zones of the La Viquita pegmatite. It occurs as small (5–20 cm diameter) nodules with rough surfaces

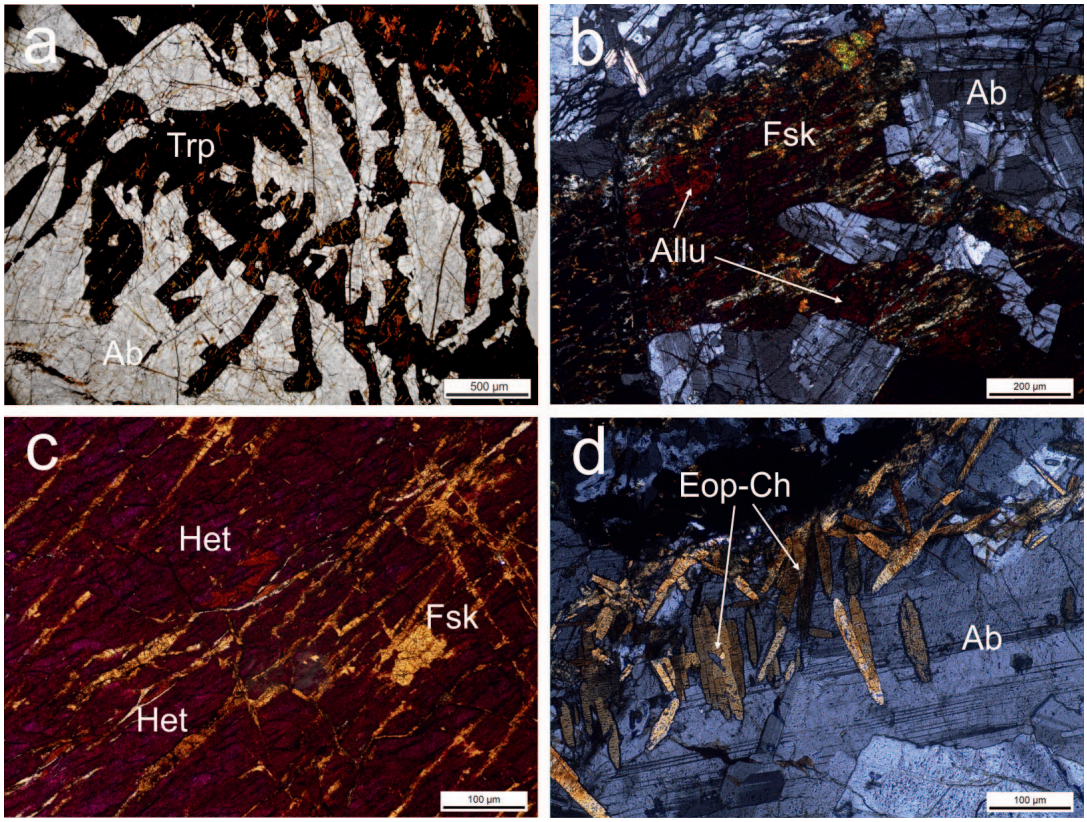

FIG. 3. Photomicrographs of different assemblages of phosphates from the La Viquita pegmatite. (a) Dendritic triphylite (Trp) partially altered and included in albite (Ab) and viewed with parallel nicols. (b) Ferrisicklerite (Fsk) after dendritic triphylite and alluaudite (Allu) viewed with crossed nicols. (c) Close-up view of triphylite totally replaced by ferrisicklerite and heterosite (Het). (d) Thin section in crossed nicols showing secondary prismatic crystals of childrenite–eosphorite (Eop–Ch) growing on albite in the wall zone.

resembling equidimensional rounded crystals, usually associated with K-feldspar, albite, spodumene, and quartz. These nodules are white, grayish white, cream white, or greenish yellow and are covered by a thin blackish film or some mix of white argillic material and iron oxides in the most altered samples. Under the microscope it shows polysynthetic twinning after {111} and {1$\bar{1}$1}. The fluorine content was determined in several samples using the indirect X-ray diffraction method of Černá *et al*. (1973) and it varies from 1.40 to 4.05 wt.%, corresponding to montebrasite, except in one case where F is up to 11.8 wt.% and is in the compositional field of amblygonite (Martínez 2005).

Ferrisicklerite $Li_{1-x}(Fe^{3+},Mn^{2+})(PO_4)$

Ferrisicklerite invariably replaces triphylite in a first alteration stage, giving the triphylite samples a dark brown color (Fig. 2b), up to a point where no remnants of the primary phase are visible. Ferrisicklerite itself develops, in a second stage of replacement, elongated, subparallel areas with irregular borders that partially coalesce, leaving interstitial patches of heterosite visible under the microscope (Fig. 3b, c). Later in this replacement sequence, alluaudite appears, initially in thin veinlets which progressively developed into patches with advanced replacement that irregularly and partially replaces the assemblage ferrisicklerite + heterosite (Fig. 3b). The ferrisicklerite chemical compositions are fairly homogeneous and show, in relation to the primary triphylite, a slight decrease of P and Mn, combined with a more significant loss of Mg, as well as oxidation of Fe and relatively strong leaching of Li, as shown in Table 2 and Figure 4. However, the $Fe_t/(Fe + Mn)$ ratio only shows a small decrease and the analyses of the primary and metasomatic phases plot almost together in the Mn_T–

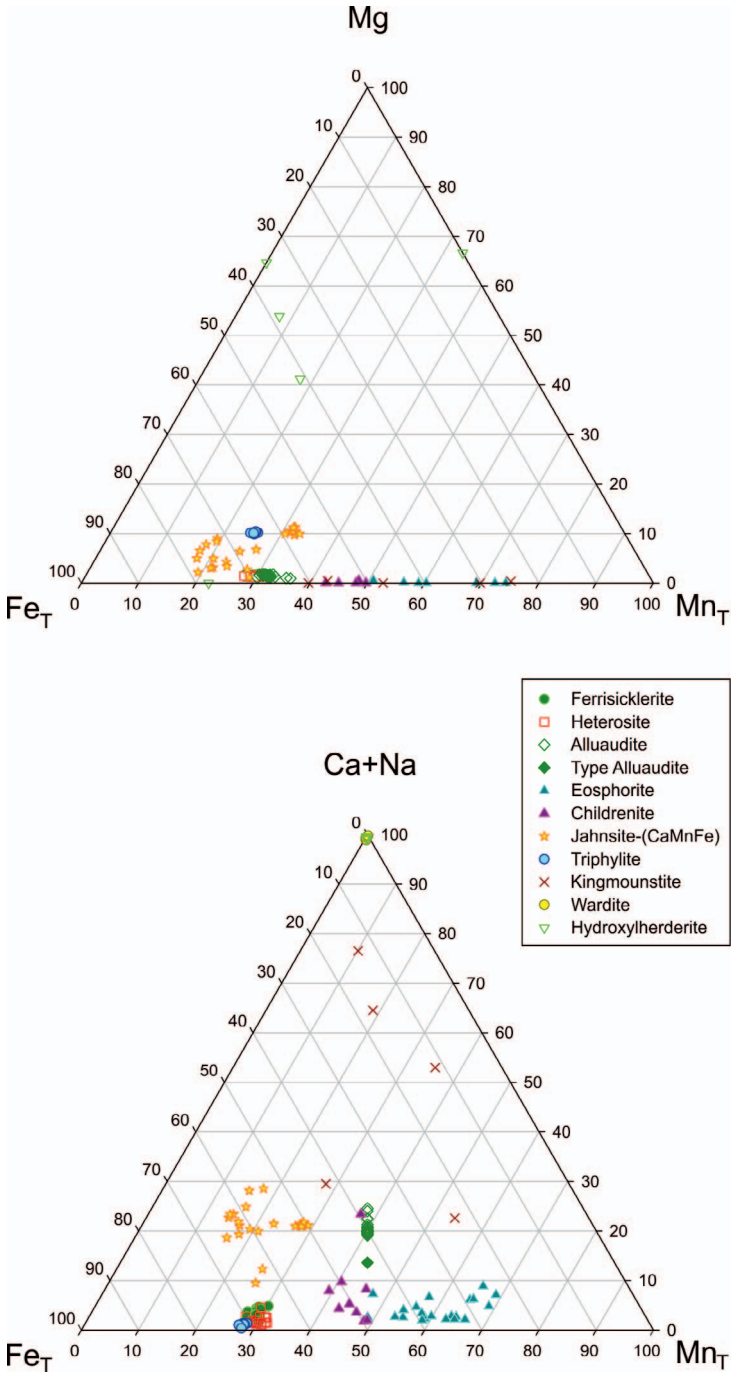

FIG. 4. Triangular diagrams. (a, top) Mn_T–Mg–Fe_T plot of the chemical composition of the phosphate assemblage from the La Viquita pegmatite. (b, bottom) Mn_T–Ca+Na–Fe_T chemical composition of the same phosphates.

TABLE 2. CHEMICAL COMPOSITIONS OF THE PHOSPHATE MINERALS FROM LA VIQUITA PEGMATITE

	Triphylite		Ferrisickler.		Heterosite		Alluaudite		Childrenite		Eosphorite		Jahnsite		Kingsmount.		Wardite		Hydroxylherd.	
	(a)		(b)		(c)		(d)		(e)		(f)		(g)		(h)		(i)		(j)	
	AVG	STD	AVG	STD	AVG	STD	AVG	STD	AVG	STD	AVG	STD	AVG	STD	AVG	STD	AVG	STD	AVG	STD
	$n = 8$		$n = 19$		$n = 15$		$n = 19$		$n = 5$		$n = 7$		$n = 23$		$n = 5$		$n = 5$		$n = 7$	
P_2O_5	46.90	0.58	45.03	0.51	46.24	0.45	44.06	1.10	30.59	0.38	30.23	1.40	33.08	1.38	29.66	1.99	35.82	0.80	43.49	0.75
SiO_2	0.34	0.12																	0.34	0.25
TiO_2	0.02	0.01																		
Al_2O_3	0.01	0.01	0.02	0.03	0.01	0.01	0.03	0.08	19.39	3.86	21.12	0.84	0.32	0.46	11.16	2.85	37.08	1.29		
Fe_2O_3*			34.92	0.84	35.23	0.77	31.73	1.59					26.62	4.80			0.10	0.05		
Mn_2O_3					15.36	0.57														
FeO	30.52	0.55					0.80	1.12	15.34	0.88	10.51	2.52	3.10	5.33	6.80	2.49			0.22	0.13
MgO	2.68	0.04	0.38	0.03	0.37	0.04	0.36	0.07	0.02	0.04	0.02	0.03	1.53	0.73	0.01	0.02	0.06	0.04	0.01	0.01
MnO	11.71	0.19	13.14	0.32			13.97	0.64	13.33	1.04	17.82	2.64	9.99	2.27	9.03	3.92	0.03	0.02	0.49	0.34
CaO	0.05	0.08	0.96	0.33	0.56	0.32	0.80	0.77	2.58	2.25	1.02	0.48	5.32	1.32	20.82	7.24	0.67	0.67	34.00	0.97
ZnO	0.12	0.04																		
SrO																			0.10	0.06
BeO																			15.44	0.28
Na_2O	0.01	0.01	0.13	0.08	0.08	0.06	6.19	0.44	0.16	0.16	0.10	0.07	1.34	0.49	1.53	0.69	6.54	0.13	0.01	0.03
K_2O			0.03	0.02	0.02	0.02	0.12	0.08	0.05	0.01	0.01	0.02	0.02	0.04	0.03	0.04	0.02	0.02		
Li_2O**	9.94	0.10	2.43	0.59																
H_2O*									15.52	0.19	15.34	0.71	17.07	3.72	19.31	1.15	17.83	0.44	5.56	0.10
F																			0.00	
Cl									0.02	0.02	0.01	0.01	0.02	0.04	0.02	0.02	0.01	0.01		
O=Cl									0.00	0.01	0.00	0.00	–0.01	0.01	0.00	0.00	0.00	0.00		
Total	102.28	1.27	97.03	0.76	97.88	0.65	98.06	1.82	96.99	1.06	96.18	0.99	98.41	4.70	98.36	6.51	98.15	2.38	99.67	1.98

TABLE 2. CONTINUED.

	Triphylite		Ferrisickler.		Heterosite		Alluaudite		Childrenite		Eosphorite		Jahnsite		Kingsmount.		Wardite		Hydroxylherd.	
	(a)		(b)		(c)		(d)		(e)		(f)		(g)		(h)		(i)		(j)	
	AVG	STD	AVG	STD	AVG	STD	AVG	STD	AVG	STD	AVG	STD	AVG	STD	AVG	STD	AVG	STD	AVG	STD
	$n = 8$		$n = 19$		$n = 15$		$n = 19$		$n = 5$		$n = 7$		$n = 23$		$n = 5$		$n = 5$		$n = 7$	
P^{5+}	0.992	0.003	1.000	0.000	1.001	0.007	3.002	0.035	1.000	0.000	1.000	0.000	4.118	0.413	5.454	0.050	2.040	0.009	0.992	0.011
Si^{4+}	0.008	0.003																	0.009	0.007
Ti^{4+}	0.000	0.000																		
Al^{3+}	0.000	0.000	0.001	0.001	0.000	0.000	0.003	0.008	0.882	0.176	0.973	0.020	0.057	0.082	2.870	0.768	2.939	0.047		
Fe^{3+}	0.100	0.002	0.689	0.020	0.678	0.015	1.921	0.082					2.935	0.525			0.005	0.003		
Mn^{3+}					0.299	0.010														
Fe^{2+}	0.637	0.008					0.054	0.076	0.496	0.023	0.344	0.081	0.384	0.668	1.247	0.497			0.005	0.003
Mg^{2+}	0.100	0.002	0.015	0.001	0.014	0.002	0.043	0.008	0.001	0.002	0.001	0.002	0.341	0.181	0.004	0.005	0.006	0.004	0.000	0.000
Mn^{2+}	0.248	0.004	0.292	0.008			0.953	0.045	0.436	0.037	0.590	0.081	1.250	0.343	1.647	0.649	0.002	0.001	0.011	0.008
Ca^{2+}	0.002	0.001	0.027	0.009	0.015	0.009	0.070	0.068	0.107	0.093	0.042	0.019	0.841	0.221	4.834	1.598	0.048	0.049	0.982	0.016
Zn	0.002	0.001																		
Sr																			0.001	0.001
Be																			1.000	0.000
Na^{+}	0.000	0.001	0.006	0.004	0.004	0.003	0.966	0.056	0.012	0.012	0.007	0.005	0.381	0.138	0.650	0.293	0.854	0.030	0.001	0.001
K^{+}			0.001	0.001	0.001	0.001	0.012	0.008	0.002	0.001	0.000	0.001	0.004	0.007	0.008	0.009	0.001	0.002		
Li^{+}	0.998	0.002	0.255	0.059																
OH^{-}									3.999	0.001	3.999	0.001	16.411	3.601	27.993	0.006	7.999	0.001	1.000	0.000
F^{-}																			0.000	
Cl^{-}									0.001	0.001	0.001	0.001	0.006	0.009	0.007	0.006	0.001	0.001		
O^{2-}									6.869	0.135	6.999	0.001	25.994	0.009	39.993	0.006	13.999	0.001	5.000	0.000
CAT SUM	2.988	0.010	2.286	0.039	2.012	0.008	7.024	0.040	2.936	0.042	2.958	0.030	10.311	1.041	16.712	0.524	5.894	0.024	3.002	0.013
AN SUM	3.985	0.010			4.000	0.000	12.000	0.000	6.870	0.134	6.940	0.038	26.000	0.000	40.000	0.000	14.000	0.000	5.000	0.000
$Fe_T/(Fe_T+Mn)$	0.720	0.004	0.702	0.009	0.694	0.011	0.675	0.015	0.532	0.029	0.368	0.087	0.735	0.067	0.996	0.006	0.662	0.386	0.29	0.21
Fe/(Fe+Mn+Mg)	0.647	0.004	0.692	0.009	0.684	0.012	0.665	0.013	0.532	0.029	0.368	0.087	0.677	0.08	0.439	0.158	0.385	0.276	0.29	0.21

* Determined by stoichiometry. (a) Li_2O calculated assuming 1(Li,Ca,Na) *apfu*; formula contents on a basis of 1(P,Si) *apfu*. (b) Formula calculated on the basis of P = 1 *apfu* following Baijot *et al*. (2014). (c) Formula contents based on 4 O *apfu*. (d) Formula contents on a basis of 7 cations and 12 O *apfu*. (e) and (f) Formula contents on a basis of 1(P) *apfu* and H_2O calculated assuming 2(OH^-,Cl^-) *apfu*. (g) Formula contents on a basis of 26 anions and 4 (P^{5+}) *apfu*. (h) H_2O calculated assuming 4(OH^-,Cl^-) *apfu*. Formula contents on a basis of 40 anions *pfu*. (i) H_2O calculated assuming 4(OH^-,Cl^-) *apfu* and formula contents on a basis of 14 anions *pfu*. (j) Formula contents based on 5 anions *pfu* assuming 1 (Be) and 1(OH^-,F^-,Cl^-) *apfu*.

$Mg–Fe_T$ and $Mn_T–Ca+Na–Fe_T$ triangular diagrams (Fig. 4a, b).

Heterosite $Fe^{3+}(PO_4)$

Heterosite occurs replacing ferrisicklerite, pseudomorphously after triphylite, mostly in the wall zone of the pegmatite, giving some irregular purple black shine to the dark nodules. In thin sections, heterosite forms elongated subparallel areas with irregular borders that coalesce and develop patches that include irregular remnants of ferrisicklerite (Fig. 3c). The chemical composition of heterosite (Table 2) shows a slightly lower Fe/Mn ratio than triphylite, almost the same as ferrisicklerite, and appreciable loss of Mg in relation to the original triphylite, plus a detectable increase of Ca *apfu* compared to triphylite (Table 2, Fig. 4a, b).

Alluaudite $(Na,Ca)(Mn,Mg,Fe^{2+})(Fe^{3+},Mn^{2+})_2(PO_4)_3$

Alluaudite occurs in the wall zone as a replacement of the original triphylite nodules; ultimately the almost complete replacement creates dull green masses associated with black Mn oxides, muscovite, and albite in irregular centimetric-sized nodules. In thin sections alluaudite is initially present in thin veinlets that become progressively more patchy with advanced replacement. It irregularly and partially replaces the assemblage ferrisicklerite (Fig. 3b) + heterosite. The chemical composition of this phase (Table 2) shows a predominance of Na at the A(1) and A(2) sites, Mn at M(1), and Fe^{3+} at M(2), firmly in the field of alluaudite (Fig. 4a, b). The nodules and dendritic occurrences of triphylite in the inner intermediate zone of the pegmatite remain mostly fresh; no alluaudite replacement was detected visually.

Childrenite $Fe^{2+}Al(PO_4)(OH)_2{\cdot}H_2O$ mm2 – eosphorite $Mn^{2+}Al(PO_4)(OH)_2{\cdot}H_2O$ mmm – ernstite $(Mn^{2+},Fe^{3+})Al(PO_4)(OH,O)_2$ 2/m

The childrenite–eosphorite series usually appears in radial fibrous clusters from 1 mm up to 1 cm that sometimes form sporadic rosettes included in albite + muscovite + quartz in the wall and outer intermediate zones. In the NE wall of the quarry, 1 cm-diameter rosettes with red centers that grade to light green in the borders of the blades were sampled (Fig. 2d). In the wall zone very thin prismatic crystals of childrenite grow on albite (Fig. 3d). Under the microscope, the color of this series varies from yellowish green to yellow and the chemical composition spans the range $Ch_{57–26}$, meaning that both members of the series are present.

In addition, X-ray diffraction diagrams of selected material from the biggest rosettes show good agreement with ernstite, the ($Mn\text{-}Fe^{3+}$) monoclinic Mn-dominant member of the group (Seeliger & Mücke 1970), and a poorer match with eosphorite. Optical determination of the extinction angle on the [001] zone shows departure from 0°, but this is not a determinative criterium since eosphorite shows similar anomalies (Hurlbut 1950). As the chemical composition of this mineral is variable along the crystals, showing parts with Fe > Mn and others with Mn > Fe, it is suggested that Fe (possibly Fe^{3+}) is the dominant cation in this slightly monoclinic structure and that the iron-dominant equivalent of ernstite is stable in nature; this would be the first known occurrence.

Jahnsite-(CaMnFe) $CaMn^{2+}Fe^{2+}{}_2Fe^{3+}{}_2(PO_4)_4(OH)_2{\cdot}8H_2O$

Jahnsite is present as 100–300 μm long, yellow-brownish prismatic crystals in samples of dendritic phosphates from the wall zone. It is associated with ferrisicklerite and alluaudite. The chemical analyses show compositions (Table 2) with variable $Fe_t/(Fe_t + Mn)$ ratios, but all the analyzed crystals correspond to the composition of jahnsite-(CaMnFe) in this populated group of chemically varied species.

Wardite $NaAl_3(PO_4)_2(OH)_4{\cdot}2H_2O$

This mineral was only identified in thin section, where it occurs as irregular colorless microscopic grains associated with oxidized prismatic childrenite crystals and opaque minerals. Its chemical composition shows, in the empirical formula, a slight excess of P and some deficit in Al, Na, and replacing cations (Table 2).

Kingsmountite $Ca_3MnFe^{2+}Al_4(PO_4)_6(OH)_4{\cdot}12H_2O$

This mineral was only identified by its chemical composition, which is relatively variable in terms of Mn/Fe ratios (Table 2). It occurs associated with jahnsite-(CaMnFe) in the most altered nodules of triphylite.

Hydroxylherderite $CaBe(PO_4)(OH)$

This mineral appears as a very late-stage phase in vugs of corroded K-feldspar crystals in the intermediate zone, close to the core of La Viquita. It occurs as subhedral 1–2 mm crystals associated with hydroxylapatite. The chemical composition indicates slight replacement of P by Si and of Fe and Mn by Ca, without showing a defined trend (Fig. 4a). Its composition and paragenesis are similar to the

hydroxylherderite from the nearby San Elías pegmatite (Galliski *et al*. 2012).

Discussion

The phosphate mineral assemblages in the La Viquita pegmatite developed in several stages at different PTX conditions. The first primary paragenesis is represented by triphylite associated with apatite, albite, and Qtz-Mc-Ms. The habit of the triphylite is dendritic to massive, and it occurs in the wall and intermediate zones. The dendritic habit can appear in several internal units (Keller 1988) and always indicates undercooling (London 2008), which supports our suggested magmatic origin for this triphylite. The $Fe_T/(Fe_T + Mn)$ ratio of the triphylite samples from different zones (0.713–0727) and its replacement phases, ferrisicklerite and heterosite, plot closely in the Mn_T–Mg–Fe_T diagram (Fig. 4a) and do not show major differences that should be present if a fractionation process was active, since their values tend to decrease in normal differentiation trends (Moore 1973, London 2008). This relative Mn_T–Mg–Fe_T invariability was probably buffered by the total budget of Fe and Mn of the pegmatite melt and the interplay of competing actions with the other Fe-Mn magmatic phases present: tourmaline, garnet, columbite-group minerals, wodginite-group minerals, and the traces of Fe content in the volumetrically very significant K-feldspar and spodumene. Regarding the initial relatively high Fe/Mn relationships of the melt, inferred from the triphylite composition, plus the pink color of the K-feldspar and the green color of the spodumene, both attributed to trace contents of Fe, it is necessary to highlight that La Viquita is a fairly peculiar pegmatite in the San Luis population. This is because the other pegmatites generally show high Mn in the phosphates, as at Cema (Roda-Robles *et al*. 2012), Santa Ana (Galliski *et al*. 2009), or Los Aleros, Amanda, and San Salvador (Hurlbut & Aristarain 1968). The Na-in-tryphilite geothermometer was not applied because the Na_2O content is always lower than 0.04 wt.% and is usually null (Hatert *et al*. 2011).

The crystallization of montebrasite begins in the intermediate zones where Li is available in quantity after crystal-melt fractionation of the pegmatite melt. Montebrasite crystallizes slightly before spodumene, competing with triphylite for the phosphorus content. This series is dominated by OH^- during most of the magmatic crystallization and fluorine only increases during the late stage. The subsolidus alteration detected in the nodules only affects them peripherally, producing an argillaceous cover. However, the microscopic crystals of wardite found associated with childrenite are possibly derivatives produced by Na metasomatism of montebrasite.

The pervasive subsolidus alteration of the pegmatitic phosphates likely results in an approximately centripetal process, because it is more developed in the wall and outer intermediate zones than in the inner units of the pegmatite. It begins with the metasomatic transformation of triphylite to ferrisicklerite produced by the oxidation of Fe and the leaching of Li and Mg, as was initially explained by Mason (1941) in his sequence and later on by Moore (1973). Subsequently, increasing oxidation of Fe and Mn produced the widespread conversion of ferrisicklerite to heterosite, in some parts following cleavage lines and in others with massive replacement. Next, alluaudite develops after the previous assemblage by dominant metasomatism of Na and minor Ca. This subsolidus transformation is produced by a late-stage process considered properly pegmatitic: the Na-metasomatism frequent in many rare-element pegmatites. At this stage wardite may develop as a byproduct of montebrasite alteration.

The next step in the phosphatic evolution is hydrothermal formation of several Fe-Mn+Ca species such as childrenite–eosphorite, kingsmountite, and jahnsite-(CaMnFe). There is some evidence suggesting that these minerals do not form in a primary magmatic stage, but in a late hydrothermal one. One clue is the habit of the fibro-radial aggregates (Fig. 2d), more typical of hydrothermally formed minerals. Another indication is the development of very thin prismatic crystals of childrenite disposed with comb textures growing on albite (Fig. 3d). Additionally, the $Fe_t/(Fe_t + Mn)$ ratios of magmatic (triphylite) and derived oxidized and leached products (ferrisicklerite, heterosite) (~0.70) and childrenite–eosphorite series (0.55–0.27) show a marked contrast, even when they coexist in the same thin section, indicating that they are not strictly contemporaneous.

The onset of Na-metasomatism could mark the transition from magmatic to hydrothermal. Meanwhile, the emergence of Ca and the increasing oxygen fugacity of the solutions could suggest the opening up of a closed system, prompting a "miniflood of Ca" (Martin & De Vito 2014). The formation of hydroxylherderite associated with hydroxylapatite in vugs in corroded K-feldspar crystals suggests that some beryl of the magmatic assemblage was reworked by very late-stage acidic fluids. Figure 5 shows the sequence of mineral formation schematically.

Conclusions

Fractionation of the primary magmatic phosphates in the La Viquita pegmatite, dominated by triphylite

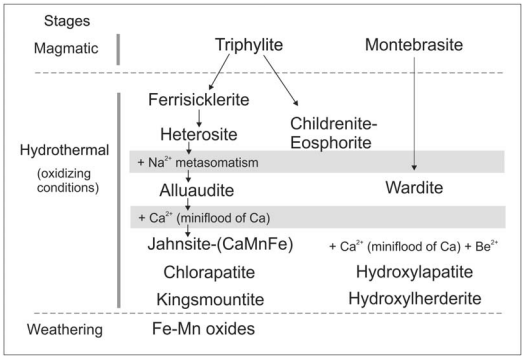

FIG. 5. Schematic diagram showing the subsolidus transformation of the primary phosphates from La Viquita pegmatite to secondary species.

and montebrasite, is minimal, possibly due to the buffering effect on transition elements of the columbite-group minerals, wodginite-group minerals, and (in trace amounts) K-feldspar and spodumene. The alteration of these phosphates develops under hydrothermal oxidizing conditions *via* a sequence of topotactic replacement of triphylite by ferrisicklerite and from it to heterosite. A Na-metasomatism process produces a partial to total transformation to alluaudite in the nodules of the wall zone. Possibly at this stage, wardite was formed in the inner zones as a secondary product of montebrasite. At the same time, minerals of the childrenite–eosphorite series (± ernstite) formed in small quantities. The subsolidus alteration process of ferrisicklerite ends with the formation of jahnsite-(CaMnFe), kingsmountite, and apatite due to the late Ca-enrichment of the hydrothermal solution. Late-stage minerals formed in cavities developed in K-feldspar by this last process comprise hydroxylherderite and hydroxylapatite. Finally, supergenic alteration of the nodules produced coatings and masses of Fe-Mn oxides widely distributed in the quarry after long exposure without mining operations.

ACKNOWLEDGMENTS

The authors are very glad to dedicate this paper as a tribute to the scientific career of Ana M. R. Neiva and her important contributions to the mineralogy and geochemistry of granitic pegmatites. This paper was made possible by financial support from CONICET and FONCYT through grants PIP 11220090100857 and PICT 22-21637, respectively, to M.A. Galliski. It also received financial support from the Spanish Ministerio de Ciencia Innovación y Universidades through research project RTI2018-094097-B-100. The authors thank Radek Škoda for the chemical analyses of the blue triphylite and Fernando Colombo for the analyses of hydroxylherderite and apatite. The authors are very grateful for careful reviews of the manuscript by Alexander U. Falster and one anonymous reviewer and for the editorial suggestions and corrections of Associate Editor Mercedes Fuertes Fuente and Editor Lee A. Groat.

REFERENCES

ANGELELLI, V. & RINALDI, C.A. (1963) Yacimientos de minerales de Li de las provincias de San Luis y Córdoba. *Comisión Nacional de Energía Atómica* **91**, (unpublished report).

BAIJOT, M., HATERT, F., & PHILIPPO, S. (2012) Mineralogy and geochemistry of phosphates and silicates in the Sapucaia pegmatite, Minas Gerais, Brazil: Genetic implications. *Canadian Mineralogist* **50(6)**, 1531–1554.

BAIJOT, M., HATERT, F., DAL BO, F., & PHILIPPO, S. (2014) Mineralogy and petrography of phosphate mineral associations from the Jocão pegmatite, Minas Gerais, Brazil. *Canadian Mineralogist* **52(2)**, 373–397.

ČERNÁ, I., ČERNÝ, P., & FERGUSON, R.B. (1973) The fluorine content and some physical properties of the amblygonite montebrasite minerals. *American Mineralogist: Journal of Earth and Planetary Materials* **58(3–4)**, 291–301.

ČERNÝ, P. & ERCIT, T.S. (2005) The classification of granitic pegmatites revisited. *Canadian Mineralogist* **43**, 2005–2026.

ČERNÝ, P., SELWAY, J.B., ERCIT, T.S., BREAKS, F.W., ANDERSON, A.J., & ANDERSON, S.D. (1998) Graftonite-Beusite in granitic pegmatites of the Superior Province: A study in contrasts. *Canadian Mineralogist* **36**, 367–376.

ČERNÝ, P., GALLISKI, M. Á., TEERTSTRA, D. K., MARTÍNEZ, V. M., CHAPMAN, R., OTTOLINI, L., & FERREIRA, K. (2011) A metastable disequilibrium assemblage of hydrous high-sanidine adulariae + low albite from La Viquita granitic pegmatite, San Luis Province, Argentina. PEG 2011, *Asociación Geológica Argentina, Serie D–Publicación Especial* **14**, 49–52.

FRANSOLET, A. M. (1980) The eosphorite–childrenite series associated with the Li-Mn-Fe phosphate minerals from the Buranga pegmatite, Rwanda. *Mineralogical Magazine* **43(332)**, 1015–1023.

FRANSOLET, A. M., KELLER, P., & FONTAN, F. (1986) The phosphate mineral associations of the Tsaobismund pegmatite, Namibia. *Contributions to Mineralogy and Petrology* **92**, 502–517.

GALLISKI, M.A., MÁRQUEZ-ZAVALÍA, M.F., ČERNÝ, P., MARTÍNEZ V.A., & CHAPMAN, R. (2008) The Ta-Nb-Sn-Ti Oxide-minerals paragenesis from La Viquita, a spodumene-bearing rare-element granitic pegmatite, San Luis, Argentina. *Canadian Mineralogist* **46**, 379–393.

Galliski, M.A., Oyárzabal, J.C., Márquez-Zavalía, M.F., & Chapman, R. (2009) The association qingheiite-beusite-lithiophilite in the Santa Ana pegmatite, San Luis, Argentina. *Canadian Mineralogist* **47(4)**, 1213–1223.

Galliski, M.Á., Černý, P., Márquez-Zavalía, M.F., & Chapman, R. (2012) An association of secondary Al-Li-Be-Ca-Sr phosphates in the San Elías pegmatite, San Luis, Argentina. *Canadian Mineralogist* **50**, 933–942.

Hatert, F., Ottolini, L., & Schmid-Beurmann, P. (2011) Experimental investigation of the alluaudite + triphylite assemblage, and development of the Na-in-triphylite geothermometer: Applications to natural pegmatite phosphates. *Contributions to Mineralogy and Petrology* **161(4)**, 531–546.

Hurlbut, C.S., Jr. (1950) Childrenite–eosphorite series. *American Mineralogist* **35**, 793–805.

Hurlbut, C.S., Jr., & Aristarain, L.F. (1968) Beusite, a new mineral from Argentina, and the graftonite – beusite series. *American Mineralogist* **53**, 1799–1814.

Keller, P. (1988) Dendritic phosphate minerals and their paragenetic relation to the silicate minerals of the pegmatites from Namibia and from the Black Hills, South Dakota, USA. *Neues Jahrbuch fur Mineralogie-Abhandlungen* **159(3)**, 249–281.

Keller, P. & von Knorring, O. (1989) Pegmatites at the Okatjimukuju farm, Karibib, Namibia Part I: phosphate mineral associations of the Clementine II pegmatite. *European Journal of Mineralogy* **1**, 567–593.

Keller, P., Fontan, F., & Fransolet, A.M. (1994) Intercrystalline cation partitioning between minerals of the triplite–zwieselite–magniotriplite and the triphylite–lithiophilite series in granitic pegmatites. *Contributions to Mineralogy and Petrology* **118**, 239–248.

Kretz, R. (1983) Symbols for rock-forming minerals. *American Mineralogist* **68**, 277–279.

London, D. (2008) Pegmatites. *Canadian Mineralogist Special Publication* **10**, 347 pp.

Martin, R.F. & De Vito, C. (2014) The late-stage miniflood of Ca in granitic pegmatites: An open-system acid-reflux model involving plagioclase in the exocontact. *Canadian Mineralogist* **52(2)**, 165–181.

Martínez, V. (2005) *Geología y Mineralogía comparativa de diferentes tipos de pegmatitas litíferas de la provincia de San Luis, Argentina*. Doctoral thesis, Inédito, Universidad Nacional de Córdoba, Córdoba, Argentina, 240 pp.

Martínez, V. & Galliski, M.A. (2000) La Viquita, Sierra de la Estanzuela, San Luis: Geología de una pegmatita de subtipo espodumeno enriquecida en óxidos de Nb-Ta-Ti-Sn. *In* Mineralogía y Metalogenia 2000 **6** (I. Schalamuk, M. Brodtkorb, & R. Etcheverry, eds.). Instituto de Recursos Minerales, Universidad Nacional de La Plata, La Plata, Argentina (295–303).

Mason, B. (1941) Minerals of the Varuträsk Pegmatite: XXIII. Some iron-manganese phosphate minerals and their alteration products, with special reference to material from Varuträsk. *Geologiska Föreningen i Stockholm Förhandlingar* **63(2)**, 117–174.

Moore, P.B. (1973) Pegmatite phosphates: descriptive mineralogy and crystal chemistry. *Mineralogical Record* **4(3)**, 103–130.

Nizamoff, J. (2006) *The Mineralogy, Geochemistry and Phosphate Paragenesis of the Palermo #2 Pegmatite, North Groton, New Hampshire*. University of New Orleans Theses and Dissertations, Paper 398, New Orleans, Louisiana, United States.

Pouchou, J. L. & Pichoir, F. (1985) "PAP" ($\phi\rho Z$) correction procedure for improved quantitative microanalysis. *In* Microbeam Analysis (J. T. Armstrong, ed.). San Francisco Press, San Francisco, California, United States (104–106).

Quensel, P. (1937) Minerals of the Varuträsk Pegmatite: I. The Lithium—Manganese Phosphates. *Geologiska Föreningen i Stockholm Förhandlingar* **59(1)**, 77–96.

Roda-Robles, E., Fontan, F., Pesquera, A., & Velasco, F. (1996) The phosphate mineral association of the granitic pegmatites of the Fregeneda area (Salamanca, Spain). *Mineralogical Magazine* **60**, 767–778.

Roda-Robles, E., Fontan, F., Pesquera, A., & Keller, P. (1998) The Fe-Mn phosphate associations from the Pinilla de Fermoselle pegmatite, Zamora, Spain: Occurrence of kryzhanovskite and natrodufrénite. *European Journal of Mineralogy* **10**, 155–167.

Roda-Robles, E., Pesquera, A., Fontan, F., & Keller, P. (2004) Phosphate mineral associations in the Cañada pegmatite (Salamanca, Spain): Paragenetic relationships, chemical compositions, and implications for pegmatite evolution. *American Mineralogist* **89(1)**, 110–125.

Roda-Robles, E., Vieira, R., Pesquera, A., & Lima, A. (2010) Chemical variations and significance of phosphates from the Fregeneda-Almendra pegmatite field, Central Iberian Zone (Spain and Portugal). *Mineralogy and Petrology* **100(1–2)**, 23–34.

Roda-Robles, E., Galliski, M. A., Roquet, M. B., Hatert, F., & de Parseval, P. (2012) Phosphate nodules containing two distinct assemblages in the Cema granitic pegmatite, San Luis province, Argentina: Paragenesis, composition and significance. *Canadian Mineralogist* **50(4)**, 913–931.

Seeliger, E. & Mücke, A. (1970) Ernstit, ein neues Mn^{2+}-Fe^{3+}-Al-phosphat und seine beziehungen zum eosphorit. *Neues Jahrbuch für Mineralogie - Monatshefte* **1970**, 289–298.

Sims, J.P., Skirrow, R. G., Stuart-Smith, P. G., & Lyons, P. (1997) Informe geológico y metalogenético de las Sierras de San Luis y Comechingones (provincias de San Luis y Córdoba), 1:250.000. Anales XXVIII, Instituto de Geología y Recursos Minerales, SEGEMAR, Buenos Aires, Argentina.

Smeds, S. A., Uher, P., Černy, P., Wise, M. A., Gustafsson, L., & Penner. P. (1998) Graftonite-beusite in Sweden: primary phases, products of exsolution, and distribution in zoned populations of granitic pegmatites. *Canadian Mineralogist* **36**, 377–394.

Tait, K. T., Hawthorne, F. C., Černý, P., & Galliski, M. A. (2004) Bobfergusonite from the Nancy pegmatite, San Luis Range, Argentina: crystal-structure refinement and chemical composition. *Canadian Mineralogist* **42(3)**, 705–716.

Wlodek, A., Grochowina, A., Golębiowska, B., & Pieczka, A. (2015) A phosphate-bearing pegmatite from Lutomia and its relationships to other pegmatites of the Góry Sowie Block, southwestern Poland. *Journal of Geosciences* **60(1)**, 45–72.

Received December 29, 2019. Revised manuscript accepted March 23, 2020.